CASE FILE
COPY

MASS DISTRIBUTION OF ORBITING MAN-MADE SPACE DEBRIS

T. Dale Bess

Langley Research Center
Hampton, Va. 23665

1. Report No. NASA TN D-8108	2. Government Accession No.	3. Recipient's Catalog No.
4. Title and Subtitle MASS DISTRIBUTION OF ORBITING MAN-MADE SPACE DEBRIS		5. Report Date December 1975
		6. Performing Organization Code
7. Author(s) T. Dale Bess		8. Performing Organization Report No. L-10477
9. Performing Organization Name and Address NASA Langley Research Center Hampton, Va. 23665		10. Work Unit No. 506-16-36-01
		11. Contract or Grant No.
12. Sponsoring Agency Name and Address National Aeronautics and Space Administration Washington, D.C. 20546		13. Type of Report and Period Covered Technical Note
		14. Sponsoring Agency Code

15. Supplementary Notes

16. Abstract

   Three ways of producing space debris have been considered, and data were analyzed to determine mass distributions for man-made space debris. The three ways were hypervelocity (3.0 to 4.5 km/sec) projectile impact with a spacecraft wall, high-intensity explosions, and low-intensity explosions. The hypervelocity projectile impacts were experiments completed recently at the Langley Research Center. Data analyzed from low-intensity and high-intensity explosions were taken from the literature.

   Two types of mass distributions prevail. For hypervelocity projectile impact of a spacecraft wall, the number of fragments fits a power law. The number of fragments for both high-intensity and low-intensity explosions fits an exponential law. However, the number of fragments produced by low-intensity explosions is much lower than the number of fragments produced by high-intensity explosions. Fragment masses down to 10^{-7} gram were produced from hypervelocity impact, but the smallest fragment mass resulting from an explosion appeared to be about 10 milligrams. Velocities of fragments resulting from hypervelocity impact were on the order of 10 meters per second, and those from low-intensity explosions were on the order of 100 meters per second. Velocities of fragments from high-intensity explosions were much higher, about 3 kilometers per second.

17. Key Words (Suggested by Author(s)) Space debris Explosions Mass distribution Fragment orbits Hypervelocity impact Spacecraft hazard	18. Distribution Statement Unclassified — Unlimited Subject Category 88

19. Security Classif. (of this report) Unclassified	20. Security Classif. (of this page) Unclassified	21. No. of Pages 30	22. Price* $3.75

MASS DISTRIBUTION OF ORBITING MAN-MADE SPACE DEBRIS

T. Dale Bess
Langley Research Center

SUMMARY

Three ways of producing space debris have been considered, and data were analyzed to determine mass distributions for man-made space debris. The three ways were hypervelocity (3.0 to 4.5 km/sec) projectile impact with a spacecraft wall, high-intensity explosions, and low-intensity explosions. The hypervelocity projectile impacts were experiments completed recently at the Langley Research Center. Data analyzed from low-intensity and high-intensity explosions were taken from the literature.

Two types of mass distributions prevail. For hypervelocity projectile impact of a spacecraft wall, the number of fragments fits a power law. The number of fragments for both high-intensity and low-intensity explosions fits an exponential law. However, the number of fragments produced by low-intensity explosions is much lower than the number of fragments produced by high-intensity explosions. Fragment masses down to 10^{-7} gram were produced from hypervelocity impact, but the smallest fragment mass resulting from an explosion appeared to be about 10 milligrams. Velocities of fragments resulting from hypervelocity impact were on the order of 10 meters per second, and those from low-intensity explosions were on the order of 100 meters per second. Velocities of fragments from high-intensity explosions were much higher, about 3 kilometers per second.

INTRODUCTION

Our near-Earth space environment has been the subject of intense studies by space scientists for many years. One such study has been concerned with the near-Earth natural meteoroid environment. Observable meteors can, in a sense, be referred to as natural space debris which have been captured by the Earth's gravitational field. Most meteoroids are small and enter the Earth's atmosphere at very high velocities. Intense heating and consequent evaporation take place, and most meteoroids are burned up in the atmosphere. By observing natural space debris with ground-based radar, ballistic cameras, and spectrographic cameras, scientists have been able to learn much about them, such as composition, orbits, fluxes, velocity distributions, near-Earth spatial densities, and hazard potential to orbiting spacecraft.

With the beginning of the space age in the late 1950's, another kind of space debris (man-made) was added to our near-Earth environment. This man-made debris includes all satellites and associated parts in near-Earth orbit. Of course, these satellites and other large parts can be tracked with ground-based radar. However, events capable of breaking up a spacecraft into a number of smaller pieces can occur. Impact of a space-craft with a meteoroid would produce small fragments. Over the past several years, a number of explosions of orbiting spacecraft have been observed. Such explosions can produce many fragments too small to be detected by ground-based radar, which is limited to tracking objects on the order of 10 centimeters and larger. Thus, it is highly probable that many undetected small fragments are in near-Earth orbit. Man-made debris is probably already more of a hazard to manned and unmanned spacecraft than natural space debris (ref. 1), and the number of man-made fragments is likely to increase.

With these thoughts in mind it becomes important to be able to estimate how many fragments, large and small, are produced when an explosion or hypervelocity impact occurs. It is obvious that ground-based radar cannot detect all fragments. There are two apparent methods of estimating the number and sizes of these small fragments. The best and direct method would be to fly an experiment which could monitor these fragments. A more practicable method, which is used in this report, is to analyze data from controlled explosion experiments and from hypervelocity impact tests of spacecraft walls. Data for hypervelocity impacts were obtained from recent experiments at the Langley Research Center, and data for spacecraft explosions are taken from the literature. This report describes the collection of data and an analysis that estimates the mass distribution of debris from these events.

SYMBOLS

A,a,b,c   constants

d   shell internal diameter, centimeters

E   energy per unit mass, joules per gram

k   constant in equations (12) and (13), $\text{grams}^{1/2}$ per $\text{centimeters}^{7/6}$

m_c mass of charge, grams

m_f mass of fragment, grams

m_s initial shell mass, grams

m_t total mass of sample, grams

N cumulative fragment number

N_h high cumulative number

N_l low cumulative number

N_o constant in equation (4)

n number of fragments from sample

R function defined in terms of charge-mass ratio (eqs. (3))

S surface area, centimeters^2

t shell thickness, centimeters

V radial velocities of fragments from high-intensity explosions, centimeters per second

w characteristic size, centimeters

μ constant used in equation (11)

ρ_c charge density, grams per centimeter^3

ρ_f density of fragment, grams per centimeter^3

ρ_s shell density, grams per centimeter^3

A bar over a symbol denotes average value.

MASS DISTRIBUTION OF FRAGMENTS PRODUCED FROM HYPERVELOCITY

PROJECTILE IMPACT WITH SPACECRAFT WALL

Description of Tests

To determine the mass distribution of fragments that result when a spacecraft wall is struck by a hypervelocity object, a simulated spacecraft wall was impacted with hyper-velocity projectiles. The experiment utilized an air-reservoir light-gas gun with a 0.22-caliber launch tube. Two such tests were made. In the first test the gas gun fired a 1.65-gram, 0.56-centimeter-diameter, steel cylinder into the spacecraft wall. The measured projectile velocity was 3.0 kilometers per second. In the second test the gas gun fired a 0.37-gram, 0.56-centimeter-diameter, aluminum cylinder into the spacecraft wall. The projectile velocity was not measured but was estimated from similar shots to be 4.5 kilometers per second.

A photograph of the simulated spacecraft wall is shown in figure 1. This particular photograph was taken after the first test had been completed. The spacecraft wall consisted of an insulated fiberglass wall in back of which were a number of electronic boxes containing resistors, capacitors, etc. to simulate a typical spacecraft wall. The simulated wall was placed on a table in front of the gas gun. A plywood enclosure surrounded the experiment to contain the debris. The events taking place during impact were photographed.

Figure 2 is a photograph from the first test showing the simulated spacecraft wall in front of the light-gas gun. Figure 2(a) was taken before firing the gun and figure 2(b) is just after firing the gun. Some fragment debris can be seen lying on the table where it fell. Figure 3 is an enlarged picture of the simulated wall showing where the projectile entered. The steel cylinder penetrated the first electronic box, deviated from its straight-line trajectory, and penetrated the fiberglass wall to the left of the second electronic box. The setup for the second test was similar to the first except that the electronic box was removed from the rear of the spacecraft wall and solar cells were mounted in front of the wall. The first test produced 13.85 grams of debris from penetration of the spacecraft wall by the steel cylinder. In the second test the aluminum cylinder penetrated one electronic box but stopped before reaching the fiberglass wall and solar cells. A total of 8.20 grams of debris was recovered from the second experiment. The floor of the plywood enclosure surrounding the experiments was covered with clean plastic. Since the fragments produced were traveling too slow to embed in the plywood, they settled on the plastic. A soft brush was used to sweep the fragments into a pile. The collected fragments were then placed in paper containers.

Fragment Velocities

Velocities of fragments produced by hypervelocity projectile impact were very low compared with the projectile velocity. The fragment velocities, measured from a 400-frame-per-second film strip that showed fragment movement, were from about 10 to 30 meters per second.

Fragment Samples

In each experiment the debris was separated into five samples according to size. The size of fragments in each sample is based upon a characteristic size of a gridded sieve which allows all fragments of that sample to pass through. If the size of fragments from a sample is known, then the number of fragments is found by dividing the total mass of the sample by the mass of a fragment from the sample.

The mesh diameters of the gridded sieves used were 0.0105 centimeter, 0.0438 centimeter, 0.1396 centimeter, and 0.5188 centimeter. The smallest sieve would pass any fragment with dimensions less than 0.0105 centimeter, that is, with a characteristic size of 0.0052 centimeter. Fragments from the second sample had dimensions between 0.0105 and 0.0438 centimeter, that is, a characteristic size of 0.0271 centimeter. Characteristic size of fragments from the third and fourth samples was 0.0917 centimeter and 0.3292 centimeter, respectively. The fifth sample consisted of only a few fragments greater than 0.5188 centimeter. Therefore, dimensions and number of fragments could be determined directly.

Shape of Fragments

Visual estimates of sample fragments show that most fragments were irregularly shaped, flat plates. About 15 percent had a length-width ratio of approximately 5. The other 85 percent had a length-width ratio of about 2. In both cases the thickness was about one-fourth the width. Some of the sample fragments are shown in figure 4.

For the longer fragments the mass is

$$m_{f,1} \approx (5w)(w)\left(\frac{w}{4}\right)\rho_f = \frac{5}{4} w^3 \rho_f$$

and the surface area is

$$S_1 \approx 2(5w)(w) + 2(5w)\left(\frac{w}{4}\right) + 2(w)\left(\frac{w}{4}\right) = 13w^2$$

where w is the characteristic size of a sample fragment that will pass through a particular mesh and ρ_f is the density of a fragment. On the basis of an average density of

various fragment materials, ρ_f is estimated to be 2 grams per centimeter[3]. For the short fragments the mass is

$$m_{f,2} \approx (2w)(w)\left(\frac{w}{4}\right)\rho_f = \frac{1}{2} w^3 \rho_f$$

and the surface area is

$$S_2 \approx 2(2w)(w) + 2(2w)\left(\frac{w}{4}\right) + 2(w)\left(\frac{w}{4}\right) = \frac{11}{2} w^2$$

The mass of a fragment based on the characteristic size of a sample is

$$m_f \approx 0.15 m_{f,1} + 0.85 m_{f,2}$$

The surface area of a fragment from a sample is

$$S \approx 0.15 S_1 + 0.85 S_2$$

The number of fragments in a sample is

$$n \approx \frac{m_t}{m_f}$$

where m_t is the total mass of a sample.

After the number of fragments from each sample has been determined, a distribution of the cumulative number of fragments with masses equal to or greater than a particular value can be obtained. The primary purpose of the following analysis is a determination of mass distribution.

Analysis

After debris from each of the two tests was separated into five samples according to size, the number of fragments in each sample was plotted as a function of fragment mass. Data from both tests showed a linear trend when plotted on full logarithmic coordinate paper. Table I gives a summary of data collected from the five samples of each test.

Data from both experiments were fitted by the method of least squares to a straight line of the form

$$Y = A + bX \tag{1}$$

6

where $Y = \ln N$ and $X = \ln m_f$, $A = \ln a$ and b are constants, and N is the cumulative number of fragments with a mass equal to or greater than m_f. In power law form, equation (1) has the form

$$N = am_f^b$$

The solutions to equation (1) are

For the first test,

$$N = 7.32m_f^{-0.80}$$

For the second test,

$$N = 4.06m_f^{-0.84}$$

The foregoing solutions, as well as experimental points for the two tests, are shown in figure 5 in which cumulative fragment number is plotted as a function of fragment mass. It can be seen that fragment number ranges from 1 to 10^6 while fragment mass ranges from about 1 gram to about 10^{-7} gram. Thus, an isolated hypervelocity projectile impact of a spacecraft wall is expected to produce a large number of fragments. Most are very small. Only about 150 fragments exist with a mass greater than 10 milligrams. Most of these small fragments cannot survive very long unless they are in very high orbits. (See ref. 2.)

MASS DISTRIBUTIONS OF FRAGMENTS FROM SPACECRAFT EXPLOSIONS

Explosion Types

Explosions which can produce fragments in space are discussed in this report and are classified as either high-intensity explosions or low-intensity explosions. In this report a high-intensity explosion is defined as one in which an explosive charge is in contact with some part of the spacecraft structure. Explosions of this type produce many small fragments which cannot be tracked with ground-based radar. A low-intensity explosion is one in which an explosive charge is not in direct contact with any spacecraft structure. Examples are (1) pressure-vessel explosions and (2) fragmentation caused by the shock wave and impacting fragments from a high-intensity explosion occurring some distance from the spacecraft. Explosion of a partially filled fuel tank, in which compressed gases from burned fuel produce fragments, would be considered a low-intensity explosion as

defined in this report. Many of the large fragments that can be tracked with ground-based radar are probably produced by these low-intensity explosions.

Fragment Velocities

Initial velocities of fragments produced by low-intensity and high-intensity explosions can range from a few meters per second to a few kilometers per second. When a metal casing filled with an explosive charge is detonated, it expands before fragmenting (in some instances up to 50 percent in radius). (See ref. 3.) The metal casing is everywhere moving outward with a velocity equal to the expansion velocity of the detonation gas in contact with the casing. For a cylindrical shell, fragments from the ends have much smaller velocities than fragments moving in a radial direction.

The expression for the radial velocities of fragments for cylindrical and spherical shells of uniform thickness is given in reference 3 and, in the present notation, is

$$V = \sqrt{2ER} \tag{2}$$

where E is the energy per unit mass for a particular explosive and R is

For a cylinder,

$$R = \frac{\dfrac{m_c}{m_s}}{1 + \dfrac{1}{2}\dfrac{m_c}{m_s}} \tag{3a}$$

For a sphere,

$$R = \frac{\dfrac{m_c}{m_s}}{1 + \dfrac{3}{5}\dfrac{m_c}{m_s}} \tag{3b}$$

The function R is given in terms of the ratio of shell mass to explosive mass (charge-mass ratio).

In reference 3, steel casings of Brinell hardness varying from 105 to 500 were tested. No significant effect of hardness on the initial velocities was found.

The six high-intensity explosions reported in this report had charge-mass ratios m_c/m_s which ranged from 1.32 to 2.57. For pentolite the energy per unit mass E is

4.2×10^3 joules per gram. Substituting these values of E and m_c/m_s into equation (2) results in fragment velocities ranging from 2.58 to 3.07 kilometers per second.

The velocities of fragments from low-intensity explosions are much smaller than velocities of fragments that are in direct contact with an explosive charge (ref. 4). Figures 5 and 6 of reference 4 show maximum velocity of side-wall fragments as a function of fuel-tank pressures from low-intensity tank explosions in which fragment pieces are accelerated by gas pressures in tanks. These fragment velocities range from about 100 to about 600 meters per second depending on tank-wall thickness.

High-Intensity Explosions

Fragment data.- To determine fragment mass distributions from high-intensity explosions, data from six thin-walled cylindrical shells subjected to high-intensity explosions were analyzed. These thin shells were analyzed because they had about the same wall thickness as the outer wall skin of many spacecraft. It is shown subsequently in this report that the number of fragments produced by these high-intensity explosions is dependent on shell thickness and internal diameter. The fragment data analyzed were taken from reference 5. The six tests are designated shots 3, 5, 9, 10, 11, and 12 to correspond to their designation in reference 5.

Data used in this report are listed in tables II and III. Table II lists pertinent physical characteristics of shell and charge. Table III lists the number of fragments occurring in various mass ranges for each shot. All six tests used SAE 1015 steel with a Brinell hardness of about 210 as a shell material. The charge used in all six shells was 50/50 pentolite.

The percent of the total shell mass recovered as fragments weighing more than 30 milligrams varied from about 52 percent for shot 3 to a high of 88 percent for shot 10. The shell and total fragment masses are shown in table II. Fragments weighing less than 30 milligrams were not recovered in reference 5. A part of the analysis in this report was to estimate the number of fragments weighing less than 30 milligrams and to establish the cut-off size below which no fragments were produced.

Distribution law.- Data in table III were used in determining a distribution law for each of the six tests. Results from fragmentation theory of shells suggest that fragment cumulative number from each test should be plotted as a function of the square root of fragment mass. (See ref. 6.) The data showed a straight-line trend when plotted on semilogarithmic coordinate paper. When fitted by least squares to a straight line, cumulative number for each test had the form

$$Y = A - cX$$

where $Y = \ln N$, $X = m_f^{1/2}$, and $A = \ln N_O$ and c are constants. In exponential form the equation is

$$N = N_O \, e^{-cm_f^{1/2}} \tag{4}$$

In equation (4), N is cumulative number of fragments with mass equal to or greater than some m_f. The mass m_f is in milligrams. Equation (4) has the same form as fragment mass distribution laws based on theoretical considerations. The results for the six tests are

$$
\left.
\begin{aligned}
N_3 &= 12\ 142\ e^{-0.44 m_f^{1/2}} \\[2em]
N_5 &= 7038\ e^{-0.24 m_f^{1/2}} \\[2em]
N_9 &= 14\ 709\ e^{-0.42 m_f^{1/2}} \\[2em]
N_{10} &= 6921\ e^{-0.23 m_f^{1/2}} \\[2em]
N_{11} &= 33\ 880\ e^{-0.36 m_f^{1/2}} \\[2em]
N_{12} &= 20\ 743\ e^{-0.31 m_f^{1/2}}
\end{aligned}
\right\} \tag{5}
$$

Numerical subscripts refer to shot number.

Total number of fragments.- The smallest fragment mass recovered from any of the tests was 30 milligrams. The total mass of fragments recovered ranged from about 52 percent to 88 percent of the total mass of the unfragmented shells. Assuming that any un-recovered fragments follow the same distribution as recovered fragments, the following procedure is used to estimate the total number of fragments produced and the minimum fragment mass that might be expected.

For an exponential law the cumulative number for a given test is given by equation (4). Taking logarithms of both sides of this equation results in

$$\ln \frac{N}{N_O} = -cm_f^{1/2}$$

The function f is defined as

$$f \equiv m_f^{1/2} = -\frac{1}{c} \ln \frac{N}{N_O}$$

The average of f between N_h and N_l (N_h and N_l are high number and low number in a given interval, respectively) is

$$\bar{f} = -\frac{1}{N_l - N_h} \int_{N_h}^{N_l} \frac{1}{c} \ln \frac{N}{N_O} \, dN \tag{6}$$

Let $N/N_O = B$; then $dN = N_O \, dB$. Equation (6) becomes

$$\bar{f} = -\frac{N_O}{c(N_l - N_h)} \int_{N_h/N_O}^{N_l/N_O} \ln B \, dB \tag{7}$$

Let the difference between N_h and N_l be unity; that is,

$$N_h - N_l = 1 \tag{8}$$

Integrating equation (7), substituting equation (8), and squaring give

$$\bar{f}^2 = \frac{1}{c^2} \left[N_h \left(\ln \frac{N_h - 1}{N_h} \right) - \ln \frac{N_h - 1}{N_O} + 1 \right]^2 \tag{9}$$

Equation (8) allows setting $\bar{f}^2$ equal to $\overline{m_f}$ with a high degree of accuracy.

Equation (9) determines the average mass for any interval. Summed over all intervals, equation (9) becomes

$$m_s = \sum_{N_h \geqq 2}^{N_h = N_O} \bar{f}^2 = \frac{1}{c^2} \sum_{N_h \geqq 2}^{N_h = N_O} \left[N_h \left(\ln \frac{N_h - 1}{N_h} \right) - \ln \frac{N_h - 1}{N_O} + 1 \right]^2 \qquad (10)$$

In the limits of this summation, N_h varies from $N_h \geqq 2$ to $N_h = N_O$ where N_O is a constant. Equation (10) can be used to estimate the combined mass of all fragments in a given distribution.

To estimate the total number of fragments produced and the minimum fragment mass, equation (10) was applied to the fragment distribution equations of six thin-walled shells subjected to high-intensity explosions. The constant (N_O and c) were derived from least-squares solutions of the data from the six experiments. When the summation was less than the original mass of the shell, the cumulative number was incremented and the summation repeated. In applying equation (10), summation was stopped when the original mass of the shell was equaled or exceeded.

A comparison of cumulative fragment number based on the minimum recovered mass given by equation (5) with cumulative fragment number based on initial shell mass given by equation (10) is presented in table IV. For shots 5, 10, and 11, cumulative numbers based on equation (5) are larger than cumulative numbers based on equation (10). For these explosions the summation of average fragment masses equaled the original shell mass at a point where the smallest fragment mass in the summation was slightly larger than the smallest fragment recovered from the data. This indicates that the least-squares solution for shots 5, 10, and 11 may have overestimated the number of larger fragments.

When plotted on semilogarithmic paper as a function of the square root of fragment mass, the cumulative number from shots 5, 10, and 11 shows appreciable scatter in the data. Data from the other three shots (3, 9, and 12) show very little scatter. As a consequence, the exponential distribution law does not represent data from shots 5, 10, and 11 as well as it does the data from shots 3, 9, and 12.

For shots 3, 9, and 12, the summation of average fragment mass equaled the original shell mass at a point where the smallest fragment mass in the summation was smaller than the smallest fragment recovered from the data. The smallest fragment mass from the summation was about 10 milligrams for shot 3. It is probable that these lower fragment masses were produced but not recovered. Assuming that the least-squares solution accurately represents the data, it appears that fragment masses on the order of 10 milligrams are the lower limit in these high-intensity explosions.

These large cumulative numbers and small fragment masses are due in part to the steel shells being very thin. In general, if thickness is increased while keeping internal diameter constant, the total number of fragments decreases. These points are discussed

in the following section in which distributions of experimental data are compared with theoretical fragment distribution laws for high-intensity explosions.

Comparison of experimental data with fragmentation theory.- The theoretical equation for cumulative number distribution for fragmentation of thin cylindrical shells due to high-intensity explosions is given in reference 6 and, in the present notation, is

$$N = \frac{m_s}{2\mu} e^{-m_f^{1/2}/\mu^{1/2}} \tag{11}$$

where m_s is the initial shell mass and μ is defined, in terms of shell thickness t, internal diameter d, and a constant k, as

$$\mu^{1/2} = kt^{5/6}d^{1/3}\left(1 + \frac{t}{d}\right) \tag{12}$$

In terms of charge-mass ratio, μ is

$$\mu^{1/2} = k\left(4 \frac{\rho_s}{\rho_c}\right)^{1/3} t^{7/6}\left(\frac{m_c}{m_s}\right)^{1/3}\left(1 + \frac{\rho_c}{4\rho_s}\frac{m_s}{m_c}\right) \tag{13}$$

where m_c is the mass of the charge, ρ_c is the charge density, and ρ_s is the shell density.

The least-squares solutions for the six shots have the same form as the theoretical equation; that is,

$$N = N_0 e^{-cm_f^{1/2}}$$

where c and N_0 are both determined. If c is equated to $(1/\mu)^{1/2}$ then $\mu = (1/c)^2$ is determined, and it is possible to determine how $m_s/2\mu$ in the theoretical equation compares with N_0 from the least-squares solution. If μ and the shell dimensions are known, sufficient information exists to determine the parameter k. For purpose of comparison, table V lists N_0 and $m_s/2\mu$ for the six shots. The quantities μ, k, and m_c/m_s are also listed.

In table V, $m_s/2\mu$ from theory is, in general, smaller than N_0 from the six shots. The calculated value of k is listed for each charge-mass ratio of the six experiments. The parameter k has a tendency to decrease with increasing charge-mass ratio.

13

For the four experiments having high charge-mass ratios (2.3 to 2.5), the average for k is 0.28. For the two explosions having low charge-mass ratios (1.3), the average for k is about 0.35. Once k is determined for any charge-mass ratio, μ is also determined. When μ is determined, the theoretical distribution equation can be used to estimate the number of fragments produced in a high-intensity explosion. One advantage of using the theoretical equation is that it applies to shells of different thicknesses. On the basis of comparison between theory and experiment, theory is conservative (at least when compared with the six experiments in this report) in that it tends to underestimate the total number of fragments produced.

Low-Intensity Explosions

The distribution law for low-intensity explosions must be obtained from experiment. Data from low-intensity explosions can usually be fitted to a distribution having the same form as the distribution law for high-intensity explosions if the mass range over which the data apply is not too large. The distribution curves of low-intensity explosions are usually not as steep. In this section, one such low-intensity explosion is analyzed.

Reference 4 lists some data from tank fragmentation of an Atlas missile. The fragmentation test produced 1337 fragments. In reference 4, only 1108 locations were considered since some locations contained more than one fragment. The data were grouped and analyzed to determine their mass distribution. Three large missile pieces ranging in mass from 136 to 445 kilograms, which were not part of the main fragmentation, were not counted. The rest of the fragments ranged in mass from about 0.5 gram to about 54.5 kilograms.

Figure 6 shows histograms taken from reference 4 that show how the fragments are distributed over various mass ranges. Figure 6(a) is the distribution over the mass range from 0 to 2270 grams. Figure 6(b) is the distribution from 0 to 54.5 kilograms. Inspection of these histograms shows that most fragments are in the lower mass range. About 91 percent of all fragments are in the mass range from 0 to 2270 grams, and 68 percent are in the mass range from 0 to 227 grams.

Figure 7 is cumulative fragment number from the histograms plotted as a function of the square root of the fragment mass. This mass distribution contains 1108 fragments. For the lower mass range where larger fragment numbers prevail, the slope becomes steeper. This occurs at a fragment mass of about 1000 grams. Thus, for the Atlas explosion, the distribution law of cumulative fragment number as a function of the square root of the fragment mass does not hold over the total fragment mass range.

Separate distribution curves taken from the histograms in figure 6 are shown in figure 8. The distribution curve for the lower fragment mass range ($0 < m_f \leq 2270$ grams) has the form

$$N = N_0 \, e^{-cm_f^{1/2}}$$

The dashed line shows how the slope of the distribution of all fragments becomes steeper for fragment masses smaller than about 1000 grams.

Figure 9 is a comparison of the distribution of the smaller fragments from figure 6(a) with a distribution curve from one of the high-intensity explosions (shot 12). One such high-intensity explosion could add about 5000 small fragments to the distribution. Figure 9 shows that the cumulative distribution of fragments from a high-intensity explosion has a much steeper slope than the fragment distribution from a low-intensity explosion. The dashed curve in figure 9 represents a superposition of the two distributions. As stated previously in the report, fragment masses on the order of 10 milligrams are about the smallest significant fragments produced in one of these high-intensity explosions.

In summary, figures 7, 8, and 9 show the nature of the distribution curve when an explosion such as the tank fragmentation of an Atlas missile occurs. The cumulative distribution curve of all fragments shows an increase in steepness at small fragment masses.

FRAGMENT DEBRIS AND SPACECRAFT HAZARD

The purpose of this report is to estimate the distribution of fragments, large and small, that are produced when hypervelocity impact or explosions occur on orbiting spacecraft. How these fragments are dispersed, how long they will survive in orbit, and the probability that an orbiting spacecraft will be hit by one of these fragments are subjects of another paper. (See ref. 1.) However, many thousands of fragments which cannot be observed are produced when a hypervelocity impact or explosion occurs. Taking into consideration the specific orbits of the spacecraft, these fragments vary in velocity relative to the spacecraft from about 4 kilometers per second to about 11 kilometers per second. With this range of velocity the untrackable fragments are capable of causing spacecraft damage. Nearly all fragments from hypervelocity impacts discussed in this report are too small to penetrate spacecraft walls but could cause other damage, such as pitting of surfaces. Fragments with masses on the order of 10 milligrams are about the smallest significant fragments produced from explosions. They travel at high velocities, and the number of fragments is high (about 5000 fragments for a high-intensity explosion). All these explosion fragments are capable of causing damage and even of penetrating spacecraft walls.

CONCLUDING REMARKS

Three ways of producing space debris have been considered and data analyzed to determine mass distributions. The three ways were hypervelocity impact of a spacecraft

wall, high-intensity explosions, and low-intensity explosions. Two types of mass distribution laws were applied to experimental results: power law and exponential law. Thousands of these debris fragments are too small to be observed but have sufficient size and velocity to cause damage to spacecraft if an encounter occurs. The presence of these small fragments should, therefore, be considered for any planned long-duration near-Earth space experiment having an orbit intersecting orbits of man-made debris.

Most fragments from hypervelocity impact with a spacecraft wall were irregularly shaped, flat plates with a thickness of about one-fourth the width. The cumulative number as a function of fragment mass fits a power law of the form $N = am_f^b$, where N is cumulative number, m_f is fragment mass, and a and b are constants. For impact of a 1.65-gram projectile, 13.85 grams of debris was produced, and fragment masses ranged from about 1 gram to 10^{-7} gram while the number of fragments ranged from 1 to 10^6. Velocities of fragments were very low (about 10 to 30 m/sec).

The number of fragments from high-intensity explosions analyzed fits an exponential law of the form $N = N_0 \, e^{-cm_f^{1/2}}$, where N_0 and c are constants. Fragment masses greater than about 10 milligrams account for all the debris mass in these high-intensity explosions. For the data analyzed, cumulative fragment number reached about 5000 while the mass of fragments ranged from about 1 gram down to 10 milligrams. Velocities of fragments from these high-intensity explosions are large, about 3 kilometers per second.

Low-intensity explosions analyzed tend to follow the same kind of distribution law as high-intensity explosions, but the slopes are not as steep. If both low-intensity and high-intensity explosions occur, a cumulative distribution curve of all fragments would become steeper at small fragment masses. These small fragments cannot be tracked, but they add significantly to the number of fragments capable of producing spacecraft damage.

Langley Research Center
National Aeronautics and Space Administration
Hampton, Va. 23665
December 2, 1975

REFERENCES

1. Brooks, David R.; Gibson, Gary G.; and Bess, T. Dale: Predicting the Probability That Earth-Orbiting Spacecraft Will Collide With Man-Made Objects in Space. [IAF Paper] A74-34, Sept.-Oct. 1974.

2. Bess, T. Dale: Size Distribution of Fragment Debris Produced by Simulated Meteoroid Impact of Spacecraft Wall. Eighth Conference on Space Simulation, NASA SP-379, 1975, pp. 575-587.

3. Gurney, Ronald W.: The Initial Velocities of Fragments From Bombs, Shell, and Grenades. Rep. No. 405, Ballistic Res. Lab., Aberdeen Proving Ground, Sept. 14, 1943. (Available from DDC as AD 36 218.)

4. Edwards, J. R.: Range Safety Considerations Related to Atlas Tank Fragmentation for the Penetration Aids Program for PMR. GD/A63-0048 (Contract No. AF 04(647)-453), General Dynamics/Astronautics, May 16, 1963. (Available from DDC as AD 501 750.)

5. Eyster, E. H.: Controlled Fragmentation of Thin Cased Munitions. OSRD Rep. No. 5630, Div. 8, Natl. Def. Res. Comm., Jan. 15, 1946. (Available from DDC as AD 31 320.)

6. Gurney, Ronald W.: The Mass Distribution of Fragments From Bombs, Shell and Grenades. Rep. No. 448, Ballistic Res. Lab., Aberdeen Proving Ground, Feb. 7, 1944. (Available from DDC as AD 36 137.)

TABLE I. - SUMMARY OF DATA FROM IMPACT TESTS

Sample	Total sample mass, m_t, g	Mass of fragment, m_f, g	Characteristic size of fragment, w, cm	Number of fragments, n	Surface area of fragment, S, cm^2
First test					
1	0.33	1.7×10^{-7}	5.2×10^{-3}	1.9×10^{6}	1.8×10^{-4}
2	.80	2.4×10^{-5}	2.7×10^{-2}	3.3×10^{4}	4.8×10^{-3}
3	1.90	9.5×10^{-4}	9.2×10^{-2}	2.0×10^{3}	5.6×10^{-2}
4	2.90	4.4×10^{-2}	3.3×10^{-1}	6.6×10^{1}	7.2×10^{-1}
5	7.92	8.8×10^{-1}	9.0×10^{-1}	9.0×10^{0}	5.3×10^{0}
Second test					
1	0.30	1.7×10^{-7}	5.2×10^{-3}	1.7×10^{6}	1.8×10^{-4}
2	.60	2.4×10^{-5}	2.7×10^{-2}	2.5×10^{4}	4.8×10^{-3}
3	1.50	9.5×10^{-4}	9.2×10^{-2}	1.6×10^{3}	5.6×10^{-2}
4	3.30	4.4×10^{-2}	3.3×10^{-1}	7.5×10^{1}	7.2×10^{-1}
5	2.50	5.0×10^{-1}	7.4×10^{-1}	5.0×10^{0}	3.6×10^{0}

TABLE II.- DIMENSION AND WEIGHT DATA FOR SHELLS AND EXPLOSIVE CHARGE

Shot	Shell wall thickness, t, cm	Shell internal diameter, d, cm	Shell mass, m_s, g	Charge mass, m_c, g	Charge-mass ratio, m_c/m_s	Total fragment mass recovered, g	Number of fragments recovered
3	0.10	4.4	105.6	261.2	2.5	54.9	856
5	.17	4.4	193.4	256.3	1.3	165.7	1230
9	.10	4.4	109.9	253.9	2.3	73.5	1052
10	.17	4.4	193.1	254.1	1.3	170.0	1276
11	.13	6.7	346.5	890.6	2.6	252.5	2710
12	.14	6.7	352.6	890.6	2.5	254.0	2772

TABLE III.- NUMBER OF FRAGMENTS OCCURRING IN VARIOUS MASS RANGES

Mass range, mg	Mass of fragment, m_f, mg	Number of fragments for —					
		Shot 3	Shot 5	Shot 9	Shot 10	Shot 11	Shot 12
30.0 to 40.0	35.0	248	93	266	147	496	497
40.0 to 53.1	46.5	224	177	253	163	512	518
53.1 to 70.6	61.8	138	148	187	183	427	481
70.6 to 93.9	82.2	112	150	137	150	378	378
93.9 to 124.8	109.3	79	176	106	157	305	336
124.8 to 166.1	145.4	35	174	56	129	243	230
166.1 to 220.8	193.4	10	119	31	158	179	160
220.8 to 293.7	257.2	6	95	11	79	104	102
293.7 to 390.6	342.1	3	52	3	60	44	43
390.6 to 519.6	455.1	0	26	2	24	19	17
519.6 to 691.0	605.3	1	15	0	17	2	7
691.0 to 919.0	805.0	0	2	0	7	1	3
919.0 to 1222	1070.5	0	3	0	1	0	0
1222 to 1626	1424.0	0	0	0	1	0	0

TABLE IV.- FRAGMENT CUMULATIVE NUMBER FROM HIGH-INTENSITY EXPLOSIONS

Shot	Cumulative number based on recovered mass (eqs. (5))	Minimum fragment mass recovered, mg	Cumulative number based on initial shell mass (eq. (10))	Minimum fragment mass calculated, mg
3	1083	30	3229	10
5	1900	30	1525	42
9	1469	30	1924	24
10	1914	30	1357	48
11	4801	30	4197	30
12	3830	30	4756	24

TABLE V.- COMPARISON OF THEORETICAL AND
EXPERIMENTAL PARAMETERS

Shot	N_O	$m_S/2\mu$	μ, g	k, $g^{1/2}/cm^{7/6}$	m_c/m_S
3	12 142	10 283	0.00513	0.30	2.5
5	7 038	5 525	.01750	.34	1.3
9	14 709	7 919	.00565	.31	2.3
10	6 921	5 318	.01815	.35	1.3
11	33 880	22 047	.00786	.24	2.6
12	20 743	16 790	.01050	.28	2.5
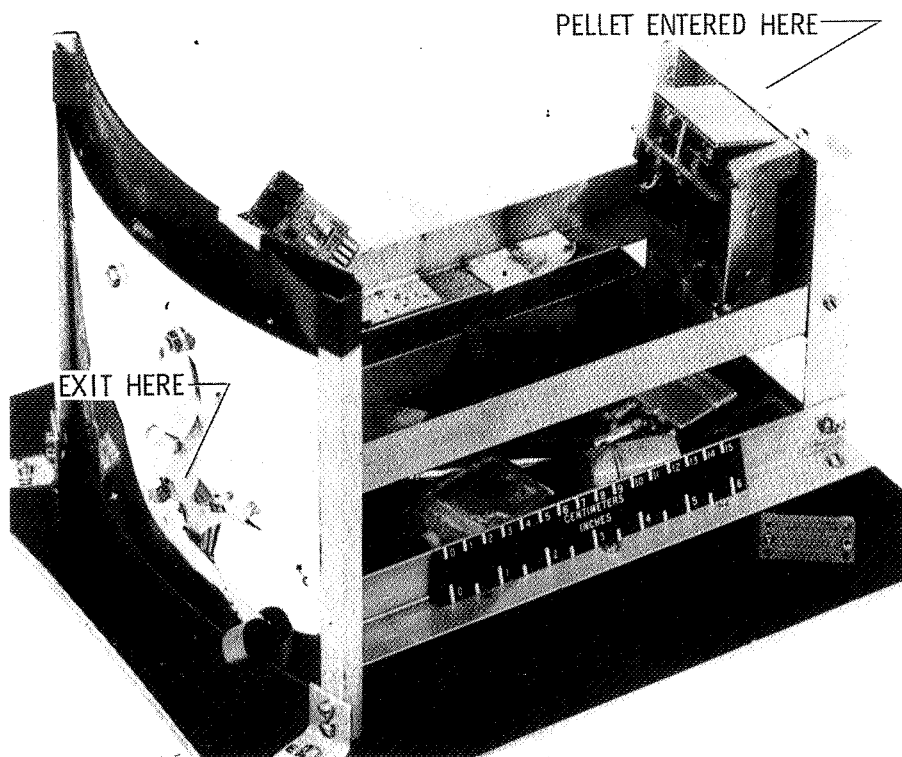
L-72-7332.1

Figure 1.- Simulated spacecraft wall.
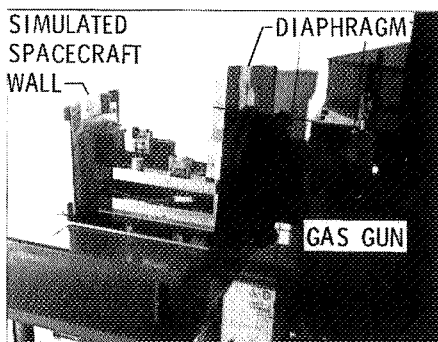
(a) Before firing the gun.
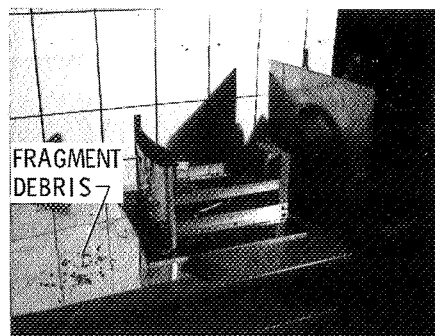
L-75-251

(b) After firing the gun.

Figure 2.- Spacecraft wall in front of gas gun.
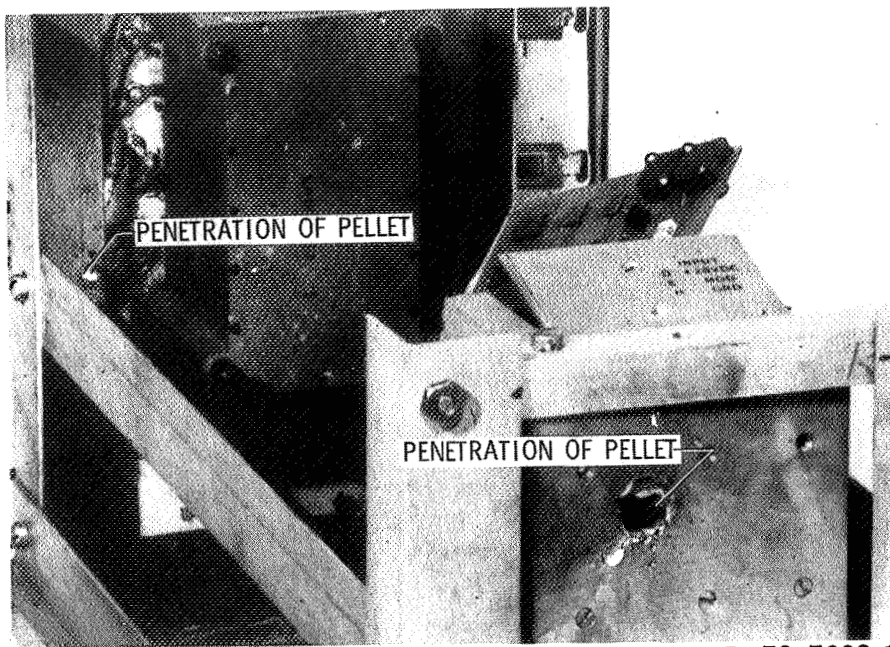
L-72-7882.1

Figure 3.- Spacecraft wall showing pellet penetration.
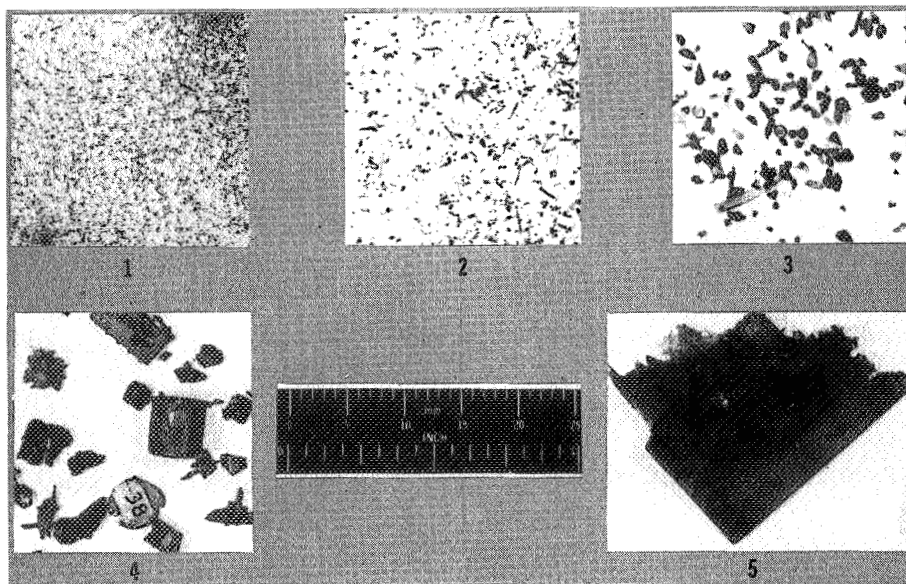
L-75-252
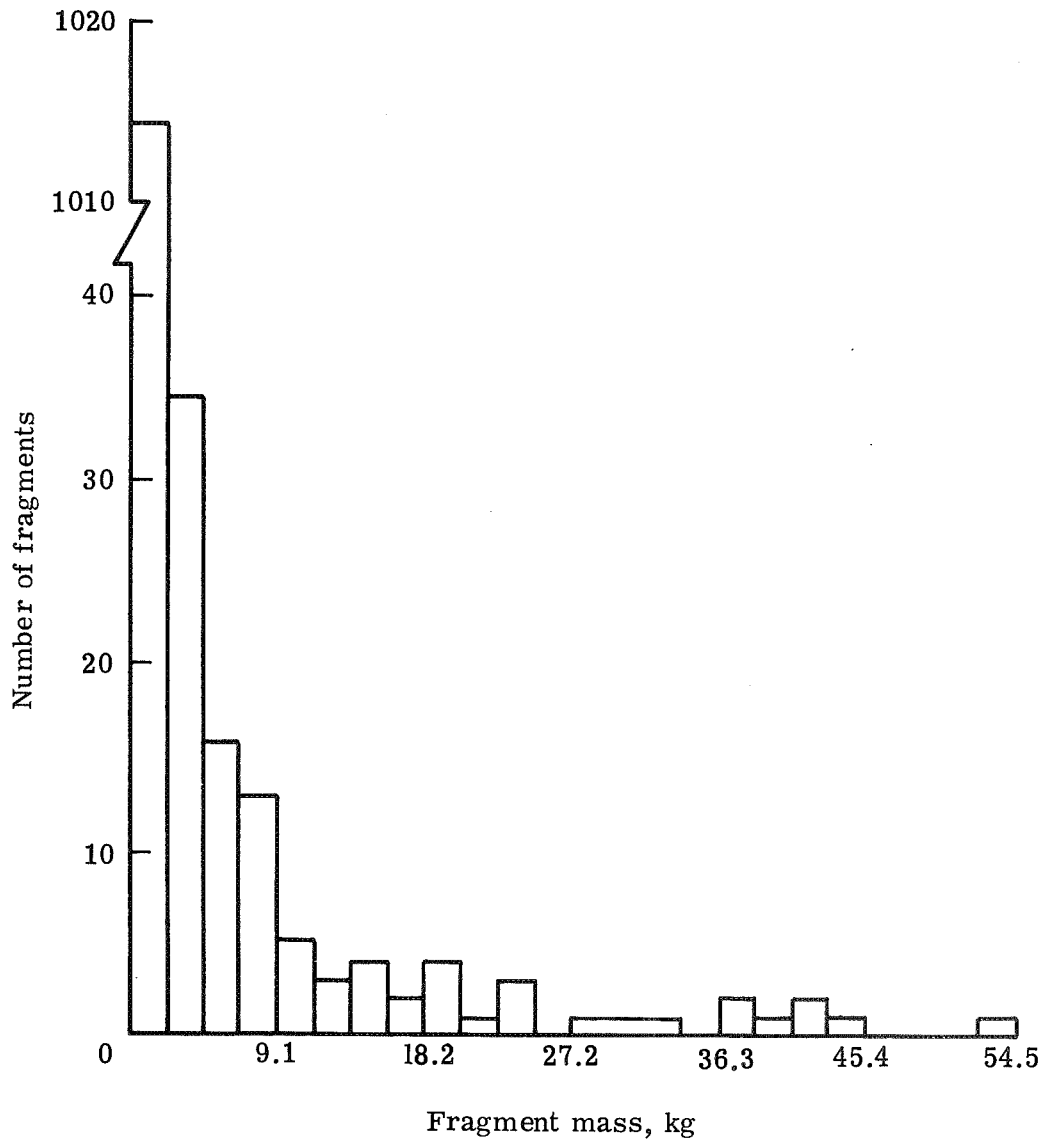
Figure 4.- Size of fragments from five samples.
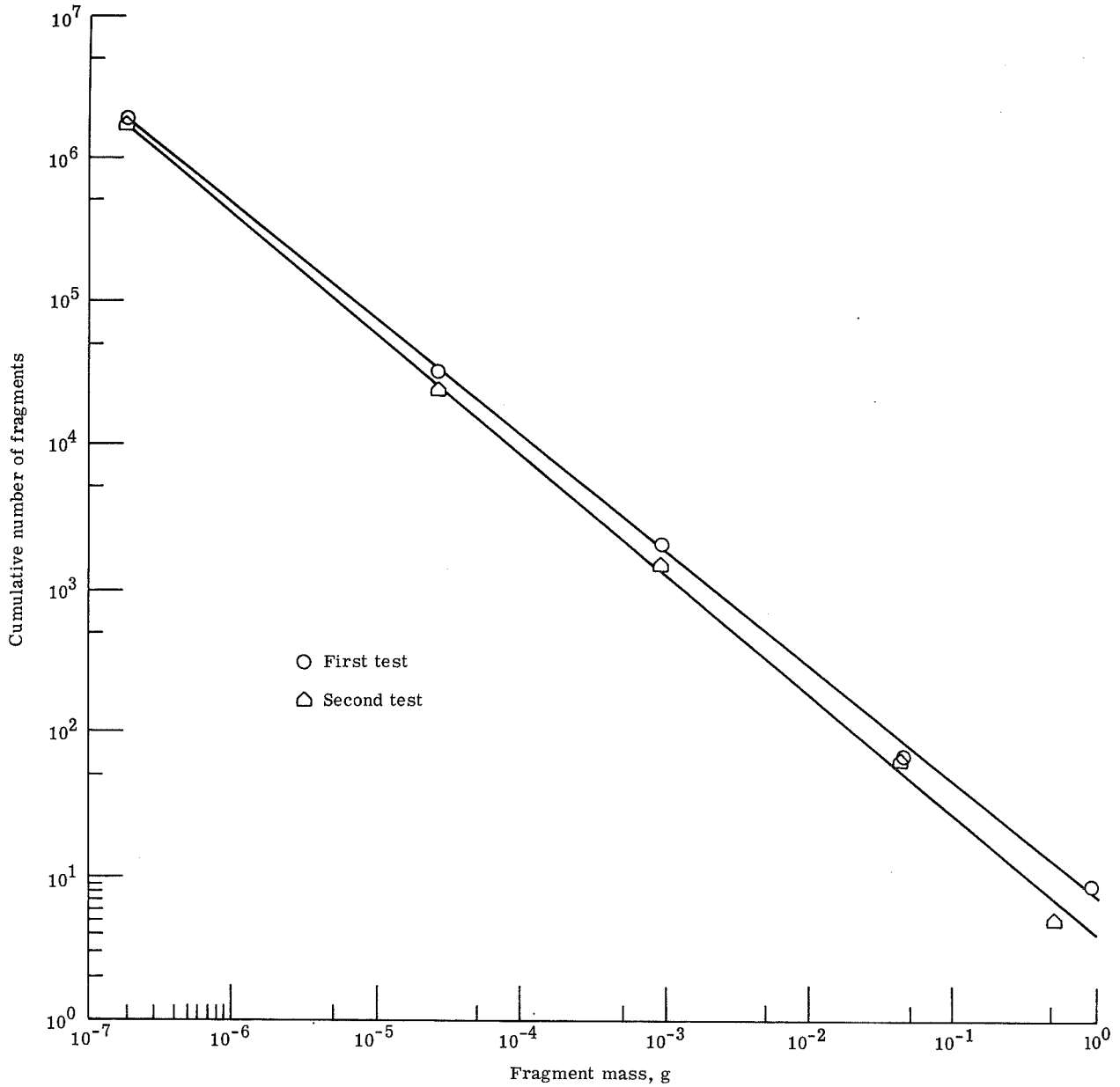
Figure 5.- Cumulative fragment mass distribution from meteoroid impact of spacecraft wall.
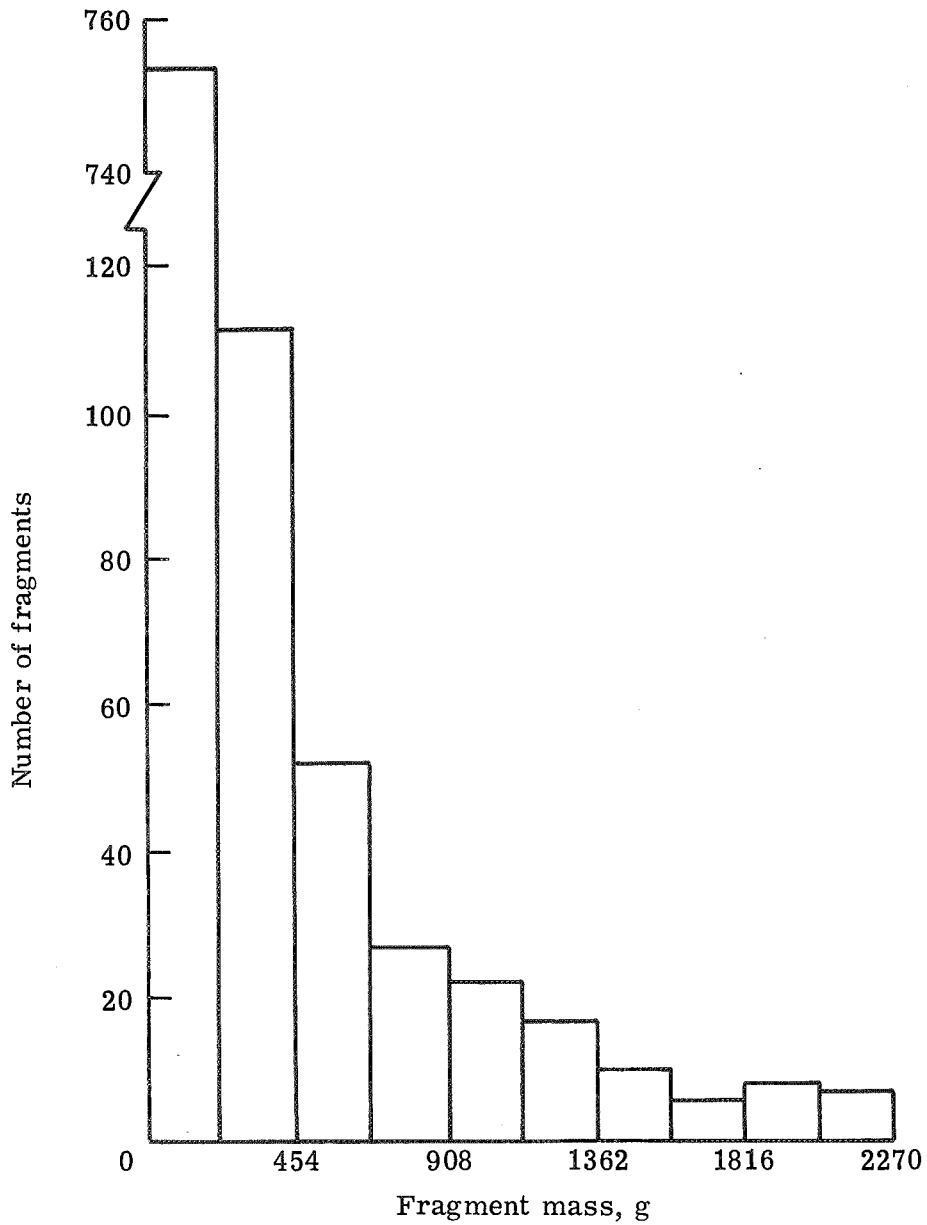
(a) Fragments with mass less than 2270 grams.

Figure 6.- Mass distribution of fragments from tank explosion from Atlas missile.

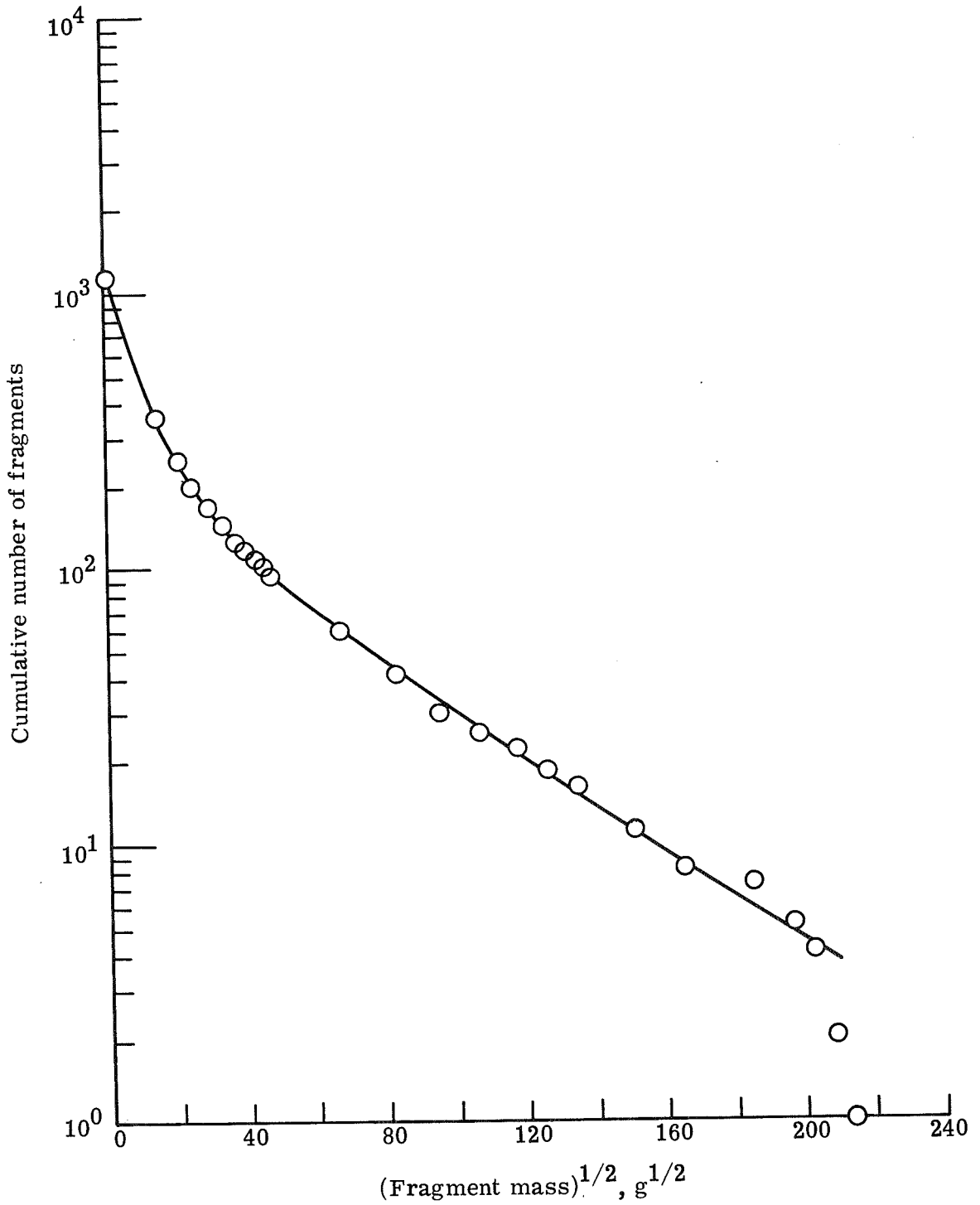(b) Fragments with mass less than 54.5 kg.

Figure 6.- Concluded.

Figure 7.- Cumulative mass distribution of fragments from explosion of tank from Atlas missile.
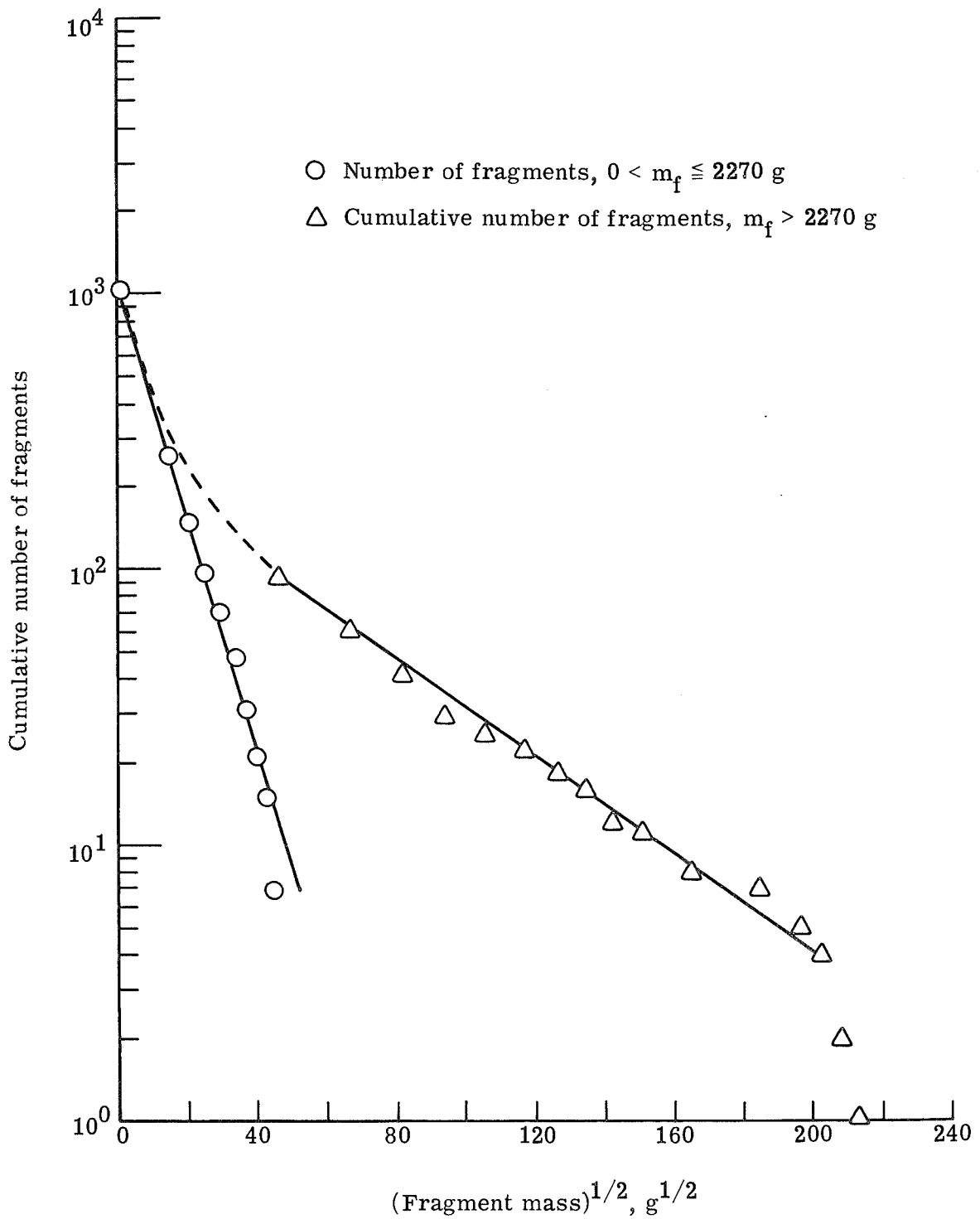
Figure 8.- Distribution curves for mass ranges from 0.5 to 2270 grams and from 2.270 to 45 kilograms.
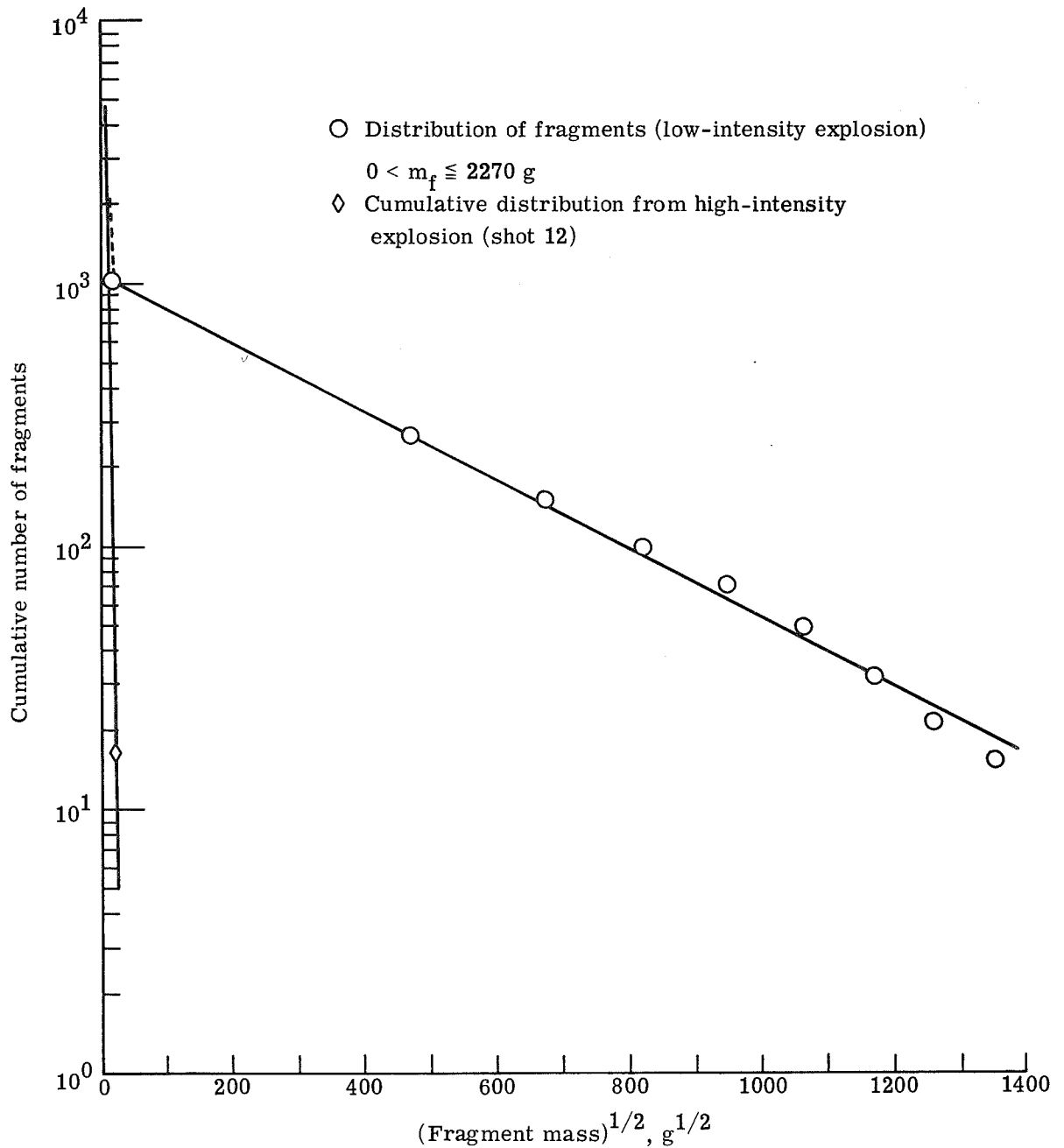
Figure 9.- Mass distributions of fragments from a high-intensity explosion and a low-intensity explosion in the low mass range.

"*The aeronautical and space activities of the United States shall be conducted so as to contribute . . . to the expansion of human knowledge of phenomena in the atmosphere and space. The Administration shall provide for the widest practicable and appropriate dissemination of information concerning its activities and the results thereof.*"
—NATIONAL AERONAUTICS AND SPACE ACT OF 1958

NASA SCIENTIFIC AND TECHNICAL PUBLICATIONS

TECHNICAL REPORTS: Scientific and technical information considered important, complete, and a lasting contribution to existing knowledge.

TECHNICAL NOTES: Information less broad in scope but nevertheless of importance as a contribution to existing knowledge.

TECHNICAL MEMORANDUMS: Information receiving limited distribution because of preliminary data, security classification, or other reasons. Also includes conference proceedings with either limited or unlimited distribution.

CONTRACTOR REPORTS: Scientific and technical information generated under a NASA contract or grant and considered an important contribution to existing knowledge.

TECHNICAL TRANSLATIONS: Information published in a foreign language considered to merit NASA distribution in English.

SPECIAL PUBLICATIONS: Information derived from or of value to NASA activities. Publications include final reports of major projects, monographs, data compilations, handbooks, sourcebooks, and special bibliographies.

TECHNOLOGY UTILIZATION PUBLICATIONS: Information on technology used by NASA that may be of particular interest in commercial and other non-aerospace applications. Publications include Tech Briefs, Technology Utilization Reports and Technology Surveys.

Details on the availability of these publications may be obtained from:

SCIENTIFIC AND TECHNICAL INFORMATION OFFICE

NATIONAL AERONAUTICS AND SPACE ADMINISTRATION
Washington, D.C. 20546